CrystEngComm

Accepted Manuscript

ROYAL SOCIETY OF CHEMISTRY

www.rsc.org/crystengcomm

Effect of calcination temperature on nanoparticle morphology and its consequence on optical properties of Nd: Y_2O_3 transparent ceramics

S. Satapathy,[a, *] Anju Ahalwat,[a] Ayushi Paliwal, [b] Rashmi Singh,[a] M. K. Singh[a] and P. K. Gupta[a]

[a] Laser Materials Development & Devices Division, Raja Ramanna Centre for Advanced Technology, Indore 452013, India

[b] School of studies in Physics, Vikram University, Ujjain , India

Key words: Precipitation; nanofabrication; Optical properties; Luminescence; X-ray diffraction

Corresponding author

[*] **E- mail:** srinu73@rrcat.gov.in, srinusatapathy@gmail.com

Phone: 91 731 2488660/8658

Fax: 91 731 2488650

Abstract

The Nd(2%) doped Y_2O_3 nano powders were synthesized by precipitation method. The precipitate was calcined at various temperatures to obtain nano powders having different particle size distribution and morphology. The changes in morphology and the size distribution were studied by scanning electron microscopy and dynamic light scattering method. The pellets fabricated using these nano powders were sintered in vacuum at 1750 ^{o}C. The transparency of pellets was compared at various calcination temperatures of precipitate. The transmittance of pellets increased with increase in calcination temperature up to 900 ^{o}C and further calcinations at higher temperature reduces the transmittance of Nd: Y_2O_3 ceramics. It was observed that the transmittance is greatly dependent on the morphology and particle size distribution. Strong absorption bands were observed at 600 and 800 nm for Nd: Y_2O_3 transparent ceramic. The Judd-Ofelt parameters were calculated from the absorption spectrum and small Ω_2 value signifies less asymmetrical environment around Nd^{3+} in Y_2O_3 host lattice. The IR (840 -1400 nm) emission photoluminescence (PL) spectra confirmed that the PL peak positions do not vary with calcination temperature. Three strong emission bands at 871-957 nm, 1045-1137 nm and 1306-1379 nm are observed corresponding to $^4F_{3/2} \rightarrow {}^4I_{9/2}$, $^4F_{3/2} \rightarrow {}^4I_{11/2}$ and $^4F_{3/2} \rightarrow {}^4I_{13/2}$ transitions of Nd^{3+} ions respectively.

Introduction

The discovery of nanocrystalline materials with improved novel properties is an important turning point in material research [1] and has excellent potential in many scientific and medical applications [2]. Among nanocrystalline ceramics, oxides exhibit higher mechanical, thermal, and chemical stability and constitute a challenging candidate for biomedical and photonic applications. Y_2O_3 based laser materials have received considerable attention for laser host application over the past years due to its high thermal conductivity (27 $Wm^{-1}C$), broad range of transparency, good chemical and photostability, high laser potentialities, and relatively low phonon energies [3-7]. Doping with complementary trivalent rare earth ions i. e. Yb^{3+}, Nd^{3+} in Y_2O_3 has potential use in ceramic laser applications [8, 9] and Eu^{+3}, Er^{3+} and Sm^{3+} doped Y_2O_3 has also used in red phosphor and display applications [10-12]. Moreover Er^{+3} doped Y_2O_3 is a promising material for optical telecommunication network [13]. The main interest in four level laser host system Nd^{3+} doped Y_2O_3 is due to its low laser power output threshold, high quantum efficiency, high simulated emission cross section and its strong absorption at 808 nm and 593 nm [14]. In Nd: Y_2O_3 laser output was observed due to active Nd^{3+} ion for transitions $^4F_{3/2} – {}^4I_{11/2}$ and $^4F_{3/2} – {}^4I_{13/2}$ manifolds at wavelengths near 1.07 and 1.35 μm respectively [15].

The melting point of Y_2O_3 is ~ 2430^0 C with a structural phase transition at ~2280^0 C [16]. Thus, it is extremely difficult to grow large-size high quality Y_2O_3 single crystals. However by using ceramic fabrication technology it is possible to fabricate optical transparent grade ceramics with big size and complex structure. These ceramics exhibit transparency and thermal mechanical properties close to single crystals. It is, however, relatively easy to fabricate Y_2O_3 ceramics because the sintering temperature is about 700°C lower than the melting temperature. The process of transparent ceramics has its special requirements, especially for powder synthesis and sintering compared to conventional ceramic fabrication processes [17]. Techniques such as inert gas atomization, chemical vapour deposition, solvothermal process, forced hydrolysis, solid solution route and spray thermal composition have been reported for producing nanocrystalline Y_2O_3 ceramics. Whereas the wet chemical methods such as coprecipitation, sol gel and emulsion provide better control of homogeneity, purity and uniform particle size [18]. The ammonium sulphate addition to precipitate greatly affects the morphology of Nd: Y_2O_3 nano particles which in turn plays important role on transparency of Nd: Y_2O_3 ceramic pellets [19]. The sintering techniques used for transparent ceramics are hot pressure (HP), hot iso-pressure (HIP), vacuum sintering, spark plasma sintering (SPS) and microwave sintering.

Transparent Nd: Y_2O_3 ceramics were prepared using precipitation and vacuum sintering [20], high energy ball milling and vacuum sintering [21] & commercial powders and sintering in H_2 atmosphere [14]. In this paper we have discussed the synthesis and characterization of Nd doped Y_2O_3 (2 mol%) nanocystalline powders prepared by co-precipitation method. The precipitate was calcined at different temperatures. The transparent Nd: Y_2O_3 ceramics produced using these nanopowders were compared. We have demonstrated the effect of calcination temperature of precursor on transparency of Nd: Y_2O_3 ceramics. The Raman and spectroscopic properties of transparent ceramics were also investigated.

Experimental

The $Y(OH)_3$ precursor were prepared by co-precipitation method and the general scheme adopted is described in Fig. 1. High purity Y_2O_3 and Nd_2O_3 (Alfa Aesar make, 99.99% purity) were used as starting materials. The steps involved in preparation of Nd: Y_2O_3 nanopowders from its salts are 1) Preparation of the yttrium nitrate (mother solution), 2) normal striking of the solution, 3) filtration and washing of precipitate, 4) drying and 5) calcinations of precursor powders. The dried $Y(OH)_3$ precursor was calcined at 600, 700, 800, 900, 1000 and 1100 ^oC. The calcined powders were pressed under pressure of 150 MPa using uniaxial press. To show only effect of morphology and particle size distribution on pellet transparency, the cold isostatic press CIP was not used for pellet pressing. The effect of CIP will be studied separately. The pellets were sintered at 1750 ^oC for 3hours using a high temperature, high vacuum furnace with tungsten mesh heating element (Hind High Vacuum High temperature furnace, Hind High Vac. Co (P). Ltd., Bangalore). Finally the pellets were lapped and polished using 300nm alumina powders.

The phase and particle size of powders calcined at different temperature were determined from X-diffraction plot which was obtained Rigaku X-ray diffractometer with a Ni filtered Cu Kα radiation source and wavelength λ of the source being 1.54 A^o. The distribution of particle size in calcined Nd: Y_2O_3 powders were measured by dynamic light scattering method (DLS) using Malvern Zetastar 90 (model no-ZEN 3690) particle size analyzer. The morphology of nano particles were explored using Zeiss field emission scanning microscope (FESEM). The optical transmittance was measured using optical spectrometer (Jasco Corporation V-670). The Raman measurements of calcined powders and sintered pellets were carried out using 488 nm excitation source using LABRAM-HR spectrometer equipped with a Peltier cooled charge coupled device (CCD) detector. The typical spectral resolution was ~1cm^{-1}. The data were collected in a backscattering geometry, wherein the incident laser light was linearly polarized while the Raman signal was detected in unpolarized mode. The photoluminescence (PL) measurement of pellets at different absorption wavelength was carried out at room temperature using PL spectrometer (FLS920-s, Edinburgh Instruments Ltd.). The background excitation source used for this purpose was a 450W ozone-free Xenon arc lamp with continuous output. A calibrated photodiode and a

R928P photomultiplier are used as excitation and emission detectors in visible range. The InGaAs with integrated Lock-in steady state (NIR 300/2, G5852-23) was used to detect IR luminescence spectra.

Results and discussion

The dried precipitate obtained after titration, filtration, washing and drying was calcined at various temperatures to produce Nd: Y_2O_3 powders. Fig. 2 shows the X-ray diffraction pattern of Nd: Y_2O_3 (2 mol%) powders prepared at pH of 7. The XRD pattern of Nd: Y_2O_3 powders is in good agreement with XRD pattern of Y_2O_3 (Standard JCPDS, Card No 41- 1105) [22]. The precipitate converted to crystalline Nd: Y_2O_3 powder at 600 ^{o}C. No other phase changes detected with increase in calcination temperature. The pure Y_2O_3 belongs to cubic crystal system having space group $Ia\overline{3}$. No significant phase change was observed on Nd doping in Y_2O_3 and the structure of Nd: Y_2O_3 (2 mol%) samples was also identified to be cubic (BCC). From fig. 2 it is clear the FWHM of highest intensity peak (222) decreases with increase in calcination temperature. Debye Scherrer formula ($0.9\lambda/t \cos\theta$) was utilized to determine the crystallite size of the Nd: Y_2O_3 powders [23]. The average crystallite size of Nd: Y_2O_3 powders calcined at various temperatures is shown in table-1. The crystallite size increases with increase in calcination temperatures.

The particle size distribution was measured by DLS method. The most important point in DLS method is preparation of colloid in which nano particles are well dispersed. Normally it is very difficult to get well dispersed Nd: Y_2O_3 nano particles in proper dispersants. Due to high surface energy the nano particles of Nd: Y_2O_3 remains in group in the dispersant. We had tried to make colloids of Nd: Y_2O_3 using reported dispersant i. e. 1-methoxy 2-propanol, Isopropanol, de-ionized water but we could not able to get well dispersed colloids. Finally we prepared well dispersed colloid of Nd: Y_2O_3 using very dilute acid solution. The statistical distribution of Nd: Y_2O_3 powders calcined at various temperatures is shown in Fig. 3. The average particle size of nano powders calcined at various temperatures is shown in table 1. The average particle size and particle size distribution range increases with increase in calcination temperature.

Scanning electron micrographs of the calcined Nd doped $Y(OH)_3$ precipitate are shown in Fig. 4. At 600 ^{o}C the particles are about to take proper shape out of precipitate. Fig. 4 (a) shows a cloud of small particles without proper boundary. At 700 ^{o}C small nano particles of different shape are formed (Fig. 4 (b)). Some particles are spherical (yellow circle Fig. 4 (b)) and some are stack of flakes (red circle Fig. 4 (b)). At this calcination temperature the particles are not well separated. As the calcination temperature of precipitate increased to 800 ^{o}C the nanoparticles took proper shape and boundaries of particles are well marked (Fig. 4 (c)). But still particles are not well separated and the size distribution of particles is narrow. Fig. 4(d) shows SEM image of Nd: Y_2O_3 nano particles evolved from calcined precipitate at 900 ^{o}C. The nano particles are well separated and particles boundary are clearly visible (yellow circles of Fig. 4(d)). The particles are not purely spherical and the distribution of particle size range is wider compared to particle size distribution at 800 ^{o}C. Further increase of calcination temperature to 1000 ^{o}C, the nano particle size increases and also the size distribution range becomes larger (Fig. 4(e)). At this temperature the nano particles try to interact with each other and necking process clearly visible in Fig. 4(f).

In order to produce Nd: Y_2O_3 transparent ceramics, the pressed pellets were sintered at 1750 ^{o}C at a vacuum of ~10^{-10} bar for 3 hours. Fig. 5 shows the transparent Nd: Y_2O_3 ceramic pellets of thickness 0.8 mm. It has been observed that the calcination temperature of precursor has great effect on the transparency of Nd: Y_2O_3 ceramics. The Nd: Y_2O_3 pellets made from powders calcined at 600 ^{o}C is less transparent compared to pellets made from powders calcined at 900 °C. The transparency of pellets was increased with increase in calcination temperature from 600 °C to 900 °C. The transmission spectra of pellets made from powders calcined at various temperatures are shown in Fig. 6. The highest transmission (≈ 70 %) of Nd: Y_2O_3 ceramics is achieved for powders calcined at 900 °C. The transmittance decreases in visible region, may be due to tiny pores, grain boundaries and impurities. These unwanted pores results in scattering and refraction of visible light. The surface roughness also reduces transmittance of ceramic pellets. The pellets used for lasing action (active medium for laser) are having transparency of ~75% (without antireflection coating)[20]. The theoretical transparency of ceramic Nd: Y2O3 pellets are ~85% without Fresnel corrections (refractive index = 1.8). The achieved transparency of ~70% without Fresnel correction in our pellets is satisfactory because these pellets were not pressed with CIP (as mentioned in experimental section). But for calcination temperature greater than 900 °C the transmittance of ceramic pellets was decreased and the color of pellets turned to dark. The transmission spectra shape and absorption peak positions were not changed for pellets prepared from powders which were calcined at various temperatures. From UV cutoff (at 276 nm) of transmission spectrum the bandgap of Nd: Y_2O_3 was calculated to be 4.49 eV. This is comparable to theoretical bandgap value of Y_2O_3 i e. 4.54 eV [24].

Raman spectra of polycrystalline Nd: Y_2O_3 nanopowder and transparent pellets were recorded at room temperature to find out the possible Raman modes and to understand the structure of Nd: Y_2O_3**.** From XRD analysis it is confirmed that Nd: Y_2O_3 is body centred cubic with space group $Ia\overline{3}$. This structure is related to the fluorite structure with each Y ion located at the centre of a cube from which two of the eight nearest neighbor oxygen of the fluorite structure have been removed. The structure contains 32 cations and 48 anions. Two kinds of cations exist: 8 Y^{3+} ions are on the b sites with symmetry C_{3i} and 24 Y^{3+} ions on the d sites with point symmetry C_2 while the 48 oxygens are on the e sites with point symmetry C_1. Because the structure is body-centered, the unit cell contains the primitive structure twice, so that only eight unit formulas must be used to theoretically determine the number of vibrations. The irreducible representations for the optical and acoustical modes are:

$\tilde{A}_{op} = 4A_g + 4E_g + 14F_g + 5A_{2u} + 5E_u + 16F_u$, $\Gamma_{ac} = F_u$

where A_g, E_g, and F_g are Raman active, F_u is IR active and A_{2u} and E_u are inactive**.** On the whole, 22 Raman lines are predicted [25, 26]**.**

Fig. 7 and Fig. 8 represent the Raman spectra observed in Nd: Y_2O_3 powders and pellets are in good agreement with that observed in the literature [27]. Though 22 modes are predicted by the theory, only 11 modes were observed in Nd: Y_2O_3. This may be due to the likelihood of band overlap as observed by A. Ubaldini et. al [28]. The most intense band in the Raman spectra was observed at 376 cm^{-1} indicating a large polarizability vibration. This band is characteristic of the cubic structure and was observed in both nanopowder and transparent pellets indicating no structural change from cubic phase. It has been observed that the Raman peaks are broader for nanopowders compared to Raman peaks of transparent pellets. As the particle size decreases the phonons are confined to the small volume of the particles. This leads to relaxation of $q = 0$ rule and in turn broadens the Raman peaks. The broadening may arises due to distribution of particle size. For different particle size the strain is different resulting in different magnitude of phonon frequency and width. This again slightly broadens the Raman bands in nanopowders compared to pellets.

Fig. 9 shows the plot of absorption coefficient with variation of wavelength of Nd: Y_2O_3 transparent ceramic having maximum transmittance. The absorption coefficient was calculated from transmittance values (T_1 & T_2) of two pellets (prepared at 900 ^oC calcination conditions) of different thickness (d_1 & d_2). Using Lambert Beer's law $\alpha = \frac{1}{(d_2 - d_1)} \ln(T_1/T_2)$ the absorption coefficient was plotted with respect to wavelength. At room temperature the main absorption bands were observed at 600 and 800 nm due to $^4I_{9/2} \rightarrow {}^4G_{5/2}+{}^2G_{7/2}$ and $^4I_{9/2} \rightarrow {}^4F_{5/2}+{}^2H(2)_{9/2}$ transitions of Nd^{3+}. The absorption wave lengths in the spectrum agree well with energy levels published in the literature [14, 20, 29, 30].

The absorption cross section of Nd^{3+} is determined by the expression

$$\sigma_{abs} = 2.302\log (I_0/I)/tN \qquad (1)$$

where $\log(I_0/I)$ is optical density, N is the active ion concentration per unit volume and t is the thickness of the sample. The Nd dopants replace both site of Yttrium i. e C_2 and C_{3i}. But the no energy transfer or cross relaxation to C_{3i} sites were considered for low concentration of Nd since no magnetic dipole allowed transitions are involved in these processes [31]. Since the Nd doping percentage is less than 3%, the number of active ions is ¾ of Nd the active ion concentration per unit volume because the unit cell contains 16 formula units with 32 cations that from 24 sites of C_2 symmetry oriented parallel to <100> and 8 sites of C_{3i} symmetry, with threefold along <111> [31]. The absorption cross section at 806 and 821nm are 1.96×10^{-20} and 2.31×10^{-20} cm^2 respectively. The absorption factors of transparent ceramics are comparable to absorption factors reported earlier [14]. The oscillator strength was calculated from the absorption coefficient spectrum using Judd-Ofelt theory. We have calculated the experimental line strength $S_{\exp}^{j_i - j_f}$ from the absorption spectrum using following equation.

$$S_{\exp}^{j_i - j_f} = \frac{\int \alpha(\lambda) d\lambda}{\left(8\pi^3 \rho \bar{\lambda} e^2 / (9ch(2j_i + 1))\right) \times \left((n^2+2)^2 / 3n\right)} \qquad (2)$$

where c is the velocity of light, h is the Planck's constant, e is the charge of electron, J_i and J_f are the total angular momentum of initial and final states, ρ is the number density of Nd^{3+} ions/cm^3, $\bar{\lambda}$ is the mean wavelength, α (λ) is the linear absorption coefficient of particular absorption band, n is the refractive index of the material and the integral in the numerator is the area under the particular absorption band [32-34].

The experimental line strengths are listed in table 2. The refractive index of Nd: Y_2O_3 was calculated using converted Sellmeier equation with λ in micrometers [35].

$$n^2(\lambda) = A + \frac{B\lambda^2}{\lambda^2 - C} + \frac{D\lambda^2}{\lambda^2 - E} \qquad (3)$$

Where A= 1.000000, B= 2.577711, C = 0.000192, D= 0.39384 and E = 5.260490 are Sellmeier coefficients.

The line strength $S_{\exp}^{j_i - j_f}$ can also be expressed by

$$S_{\exp} = \sum_{t=2,4,6} \Omega_t \left| \left\langle (S,L)J \left\| U^t \right\| (S^{/},L^{/})J^{/} \right\rangle \right|^2 \qquad (4)$$

where the elements $\left\langle \left\| U^t \right\| \right\rangle$ are the doubly reduced matrix elements and found to be almost invariant to the environment and we have used the values given by Carnall et al [36]. From $S_{\exp}^{j_i - j_f}$ the Judd-Ofelt parameters Ω_t were calculated and found to be $\Omega_2 = 2.519 \times 10^{-20}$, $\Omega_4 = 2.183 \times 10^{-20}$ and $\Omega_6 = 2.122 \times 10^{-20}$ cm^2. There is wide variation in reported the Judd-Ofelt parameters Ω_t for Nd: Y_2O_3 [14, 21, 30]. But the quality factor $Q = \Omega_4/\Omega_6$ lies in the range from 0.22 to 1.5 for Nd^{3+} for several host materials [37]. In our case the quality factor was found to be 1.028 which is well agreement with reported quality factors for Nd^{3+} in Y_2O_3 [14, 21, 30]. Using Judd-Ofelt parameters the calculated line strength of each absorption band can be derived.

$$S_{cal} = \sum_{t=2,4,6} \Omega_t \left| \left\langle (S,L)J \left\| U^t \right\| (S^{/},L^{/})J^{/} \right\rangle \right|^2 \qquad (5)$$

The calculated line strength of absorption bands are listed in table 2. The root mean square deviation ΔS_{rms} is 0.0980×10^{-20} cm^2 that signifies a good fit. The value of Ω_2 reflects the asymmetry of the local environment at the Nd^{3+} ion site [38]. The weaker the value of Ω_2 shows the more centrosymmetrical nature of the ion site and the more ionic nature of the chemical bond with the ligands [39]. The Ω_2 value in our case is small compared to reported Ω_2 values for Nd: Y_2O_3 [14, 21, 30] signifies less asymmetrical environment around Nd^{3+} in Y_2O_3 host lattice.

The photoluminescence spectra at 300 K of transparent pellets are shown in Fig. 10. In the measured range we observed three emission bands 871-957 nm, 1045-1137 nm and 1306-1379 nm corresponding to $^4F_{3/2} \rightarrow {}^4I_{9/2}$, $^4F_{3/2} \rightarrow {}^4I_{11/2}$ and $^4F_{3/2} \rightarrow {}^4I_{13/2}$ transitions of Nd^{3+} ion respectively. The observed multiplet emission transitions are from the Stark levels R_1 and R_2 of the $^4F_{3/2}$ manifolds to $^4I_{9/2}(Z_{1-5})$, $^4I9_{11/2}(Y_{1-6})$ and $^4I_{13/2}(X_{1-7})$ manifolds [30]. For all pellets the position of emission peaks in the range 840 – 1400 nm are same except variation in intensities. Fig. 11 shows emission spectra of the pellet prepared using nano powders calcined at 900 ^oC excited at different wave length above and below bandgap of Nd: Y_2O_3. The IR emission spectra at various excitation wave lengths almost identical.

Using the line strength S_{cal} for each transition, the radiative decay rates, $A\ (J_i \rightarrow J_f)$, for electric dipole transitions between an excited state (J_i) and lower-lying terminal manifold (J_f) can be calculated by [30]

$$A(J_i - J_f) = \frac{64\pi^4 e^2}{3h(2J_i+1)\bar{\lambda}^3}\left[\frac{n(n^2+2)^2}{9}\right] S_{cal}(J_i - J_f) \qquad (6)$$

The radiative life time τ_r for the excited state (J^f) is calculated by

$$\tau_r = \frac{1}{\sum A(J_i \rightarrow J_f)} \qquad (7)$$

The radiative decay rate and the life time of emission lines are listed in table 3. The maximum intensity emission lines at 893, 1078 and 1356 nm corresponds to transitions $^4F_{3/2} \rightarrow {}^4I_{9/2}$, $^4F_{3/2} \rightarrow {}^4I_{11/2}$ and $^4F_{3/2} \rightarrow {}^4I_{13/2}$ respectively. The calculated radiative life time of $^4F_{3/2}$ level at 1079 was found to be 0.37 ms. The value is in well agreement with the reported value [21]. The calculated branching ratio for transitions $^4F_{3/2} \rightarrow {}^4I_{9/2}$, $^4F_{3/2} \rightarrow {}^4I_{11/2}$ and $^4F_{3/2} \rightarrow {}^4I_{13/2}$ are found to be 0.31, 0.61 and 0.07 respectively.

Conclusions

The Nd(2%):Y_2O_3 transparent ceramics were fabricated using powders prepared by co precipitation method without addition of sintering additives. The calcination temperature of precipitate was found to have great effect on morphology, particle size and particle size distribution. The transmittance increases with increase in calcination temperature up to 900 °C and for futher higher calcination temperature the transmittance of pellets reduces. The highest transmittance is observed in the pellets which were made from Nd: Y_2O_3 powders calcined at 900 °C. The transmittance of ceramic pallets depends on morphology, particle size as well as particle size distribution. Raman studies reveal that the transparent pellets have cubic structure and no structural change is observed as a result of increasing calcination temperatures. From experimental absorption line strength the Judd-Ofelt parameters for Nd:Y_2O_3 transparent ceramics were found to be $\Omega_2 = 2.519 \times 10^{-20}$, $\Omega_4 = 2.183 \times 10^{-20}$ and $\Omega_6 = 2.122 \times 10^{-20}$ cm^2. The absorption cross section at 806 nm (available diode absorption wave length) is 1.96×10^{-20} cm^2. We have observed similar photoluminescence spectra (between 840 – 1400 nm) for all excitation wave lengths above and below band gap. Three emission bands observed at 871-957 nm, 1045-

1137 nm and 1306-1379 nm corresponding to $^4F_{3/2}\rightarrow{}^4I_{9/2}$, $^4F_{3/2}\rightarrow{}^4I_{11/2}$ and $^4F_{3/2}\rightarrow{}^4I_{13/2}$ transitions of Nd^{3+} ion respectively in measured PL range. The radiative life time of $^4F_{3/2}$ level at 1079 was calculated and found to be 0.37 ms. The branching ratio for transitions $^4F_{3/2}\rightarrow{}^4I_{9/2}$, $^4F_{3/2}\rightarrow{}^4I_{11/2}$ and $^4F_{3/2}\rightarrow{}^4I_{13/2}$ were also calculated and found to be 0.31, 0.61 and 0.07 respectively.

Acknowledgements

We thank Dr. Gurvinderjit Singh and S. K. Pathak for sintering of pellets in high vacuum furnace.

Caption of figures

Fig. 1. Schematic diagram of fabrication procedure of transparent Nd: Y_2O_3 ceramics.

Fig. 2. X-ray diffraction pattern of the precipitate and Nd: Y_2O_3 powders calcined at various temperatures.

Fig. 3. Particle size distribution observed by DLS method of Nd: Y_2O_3 powders calcined at (a) 600, (b) 700, (c) 800, (d) 900, (e) 1000 and (f) 1100 ^oC.

Fig. 4. SEM micrographs showing morphology of Nd doped $Y(OH)_3$ precipitate calcined at (a) 600, (b) 700, (c) 800, (d) 900 and (e) 1000 ^oC. (f) The necking process between nano particles at 1000 ^oC.

Fig. 5. Photographs of Nd: Y_2O_3 transparent ceramic pellets prepared from powders which were calcined at various temperatures.

Fig. 6. The transmittance of Nd: Y_2O_3 transparent ceramic pellets prepared from powders which were calcined at (a) 600, (b) 700, (c) 800, (d) 900, (e) 1000 and (f) 1100 ^oC.

Fig. 7. Raman spectra of Nd: Y_2O_3 powders calcined at (a) 600, (b) 700, (c) 800, (d) 900, and (e) 1100 ^oC.

Fig. 8. Raman spectra of Nd: Y_2O_3 transparent ceramic pellets prepared from powders which are calcined at (a) 600, (b) 700, (c) 800, (d) 900, (e) 1000 and (f) 1100 ^oC.

Fig. 9. Absorption spectrum of Nd: Y_2O_3 transparent ceramic pellet prepared from powder which was calcined at 900 ^oC.

Fig. 10. Room temperature photoluminescence spectra of Nd: Y_2O_3 transparent ceramic pellets prepared from powders calcined at (a) 600, (b) 700, (c) 800, (d) 900, (e) 1000 and (f) 1100 ^oC at excitation wavelength 593 nm.

Fig. 11. Photoluminescence spectra of Nd: Y_2O_3 transparent ceramic pellet (calcined at 900 ^oC) at various excitation wave lengths above and below band gap.

References

1 C. Suryanarayana and C. C. Koch, Hyperfine interactions, 2000, 130, 1.

2 B. I. Lee, L. Qi, and T. Copeland, J. Ceramic Proc. Res., 2005, 6, 31.

3 J. Kong , D.Y. Tang, J. Lu and K. Ueda, Appl. Phys. B, 2004, 79, 449.

4 K. Petermann, G. Huber, L. Fornasiero, S. Huch, E. Mix, V. Peters, S. Basun, J. Lumin., 2000, 973, 87.

5 L. Laversenne, Y. Guyot, C. Goutaudier, G. Boulon and M. T. Cohen-Adad, Opt. Mater., 2001, 59, 16.

6 N. Yamada, S. Shionoya and T. Kushida, J. Phys. Soc. Japan, 1972, 32, 1577.

7 W. J Kim, J. Y. Park, S. J. Oh, Y. S. Kim, G. W. Hong, I. H. Kuk , J. Mater. Sci. Lett., 1999, 18, 411.

8 J. Kong, J. Lu, K. Takaichi, T. Uematsu, K. Ueda, D. Y. Tang, D. Y. Shen, H. Yagi, T. Yanagitani and A. A. Kaminskii, Appl. Phys. Lett., 2003, 82, 2556.

9 J. Lu, Junhua Lu, T. Murai, K. Takaichi, T. Uematsu, K. Ueda, H. Yagi, T. Yanagitani and A. A. Kaminski, Jpn. J. Appl. Phys., 2001, 40, L1277.

10 N. Vu, T. K. Anh, G-C. Yi, W. Strek, J. Lumin., 2007, 122, 776.

11 F. Vetrone, J. C Boyer, J. A. Capobianco, A. Speghini, M. Bettinelli, J. Phys. Chem. B, 2003, 107, 1107.

12 C. A. Kodaira, R. Stefani, A.S. Maia, M.C.F.C. Felinto and H.F. Brito, J. Lumin., 2007, 127, 616.

13 C. Strohhofer, A. Polman, J. Appl. Phys., 2001, 90, 4314.

14 H. Zhou, Q. Yang, J. Xu and H. Zhang, J. Alloy Compd., 2009, 471, 474-476.

15 J. Stone and C. A. Burrus, J. Appl. Phys., 1978, 49, 2281-2287.

16 A. A. Kaminskii; Crystalline lasers: Physical Processes and operating schemes. Boca Raton: CRC Press Inc; 1996.

17 S. F. Wang, J. Zhang, D. W. Luo, F. Gu, D. Y. Tang, Z. L. Dong, G. E. B. Tan, W. X. Que, T. S. Zhang, S. Li and L. B. Kong, Progress in Solid State Chemistry, (2013), http://dx.doi.org/10.1016/j.progsolidstchem.2012.12.002.

18 Z. Huang, X. Sun, Z. Xiu, S. Chen and C-T. Tsai, Materials Lett., 2004, 58, 2137.

19 H. Qin, H. Liu, Y. Sang, Y. Lv, X. Zhang, Y. Zhang, T. Ohachi and J. Wang, CrystEngComm., 2012, 14, 1783-1989.

20 A. Fukabori, M. Sekita, T. Lkegami, N. Lyi and T. Komatsu, M. Kawamura and M. Suzuki, J. Appl. Phys., 2007, 101, 043112.

21 X. Hou, S. Zhou, T. Jia, H. Lin and H. Teng, J. Lumin., 2011, 131, 1953-1958.

22 L. Wen, X. Sun, Q. Lu, G. Xu and X. Hu, Optical materials , 2006, 29, 239.

23 B. D. Cullity and S. R. Stock, Element of X –ray Diffraction, 3rd ed. New Jersey: Prentice-Hall; 2001.

24 Y. N. Xu, Z. Gu and W. Y. Ching, Phys. Rev. B, 1997, 56, 14993-15000.

25 Y. Replin, C. Proust, E. Husson and J. M. Beny, J. Solid State Chem., 1995, 118, 163.

26 B. W. White and V. G. Kermidas, Spectrochim. Acta, 1972, 28A, 501.

27 J. C. Panitz, J. C. Mayor, B. Grob and W Durish, 1998, 303, 340.

28 A. Ubaldini and M. M. Carnasciali, J. Alloy Compd., 2008, 454, 374.

29 J. Lu, J. Lu, T. Murai, K. Takaichi, T. Uematsu, K. Ueda, H. Yagi, T. Yanagitani and A. Kaminskii, Jpn. J. Appl. Phys., 2001, 40, L1277-L1279.

30 K. L. Nash, R. C. Dennis, J. B. Gruber and D. K. Sardar, J. Appl. Phys., 2009, 105, 033102.

31 A. lupei, V. Lupei, T. Taira, Y. Sato, A. Ikesue and C. Gheorghe, J. Lumin., 2003, 102, 72-76.

32 B.R. Judd, Phys. Rev., 1962, 127, 750

33 G. S. Ofelt, J. Chem. Phys., 1962, 37, 511.

34 W. F. Krupke, IEEE J. Quantum Electron., 1974, 10, 450.

35 B. M. Walsh, J. M. McMohan, W. C. Edwards, N. P. Barnes, R. W. Equall and R. L. Hutcheson, J. Opt. Soc. Am. B, 2002, 19, 2893-2903.

36 W. T. Carnall, P. R. Fields, B. G. Wybourne, J. Chem. Phys., 1965, 42, 3797.

37 R. C. Powell, Physics of Solid state Laser materials, Springer, New York, 1998.

38 J. H. Choi, A. Margaryan, A. Margaryan, F. G. Shi, J. lumin., 2005, 114, 167-177.

39 C. K. Jorgensen, R. Reisfeld, J. Less-Common Met., 1983, 93, 107.

TABLE 1: Particle size of Nd: Y_2O_3 at various calcination temperatures

Calcination temperature of Nd: Y_2O_3 precipitate (°C)	**Crystallite size from XRD $t = 0.9\,\lambda/B\cos\theta$ (in nm)**	**Particle size using DLS (in nm)**
600	~31	49
700	~48	68
800	~63	79
900	~82	94
1000	~105	129
1100	~243	208

TABLE 2: Measured and calculated absorption line strengths of Nd: Y_2O_3 transparent ceramic pellet

Transition from $^4I_{9/2}$	$\bar{\lambda}$ **(nm)**	S_{exp} **(10^{-20} cm^2)**	S_{cal} **(10^{-20} cm^2)**
$^2L_{15/2}$, $^4D_{1/2}$, $^2I_{11/2}$	*360*	*1.149*	*1.101*
$^2P_{1/2}$	*446*	*0.008*	*0.009*
$^2K_{15/2}$, $^2D_{3/2}$, $^2G_{9/2}$, $^4G_{11/4}$	*480*	*0.165*	*0.166*
$^4G_{7/2}$	*539*	*0.912*	*0.912*
$^2G_{7/2}$, $^4G_{5/2}$	*590*	*3.88*	*3.881*
$^4S_{3/2}$, $^4F_{7/2}$	*752*	*1.499*	*1.602*
$^4F_{5/2}$, $^2H_{9/2}$	*813*	*1.647*	*1.455*
$^4F_{3/2}$	*890*	*0.617*	*0.598*

TABLE 3: Emission characteristic of Nd: Y_2O_3 transparent ceramic pellets

Transition	**Transition between stark levels**	$\bar{\lambda}$ **(nm)**	S_{cal} $(10^{-20}\ cm^2)$	$A(J_i\text{–}J_f)$ (s^{-1})
$^4F_{3/2}\rightarrow {}^4I_{9/2}$	R_2-Z_1	877.50	0.4424	304.239
	R_1-Z_1	893.06	0.4424	288.567
	R_2-Z_1	912.71	0.4424	270.274
	R_2-Z_4	928.27	0.4424	256.868
	R_1-Z_5	945.88	0.4424	242.741
$^4F_{3/2}\rightarrow {}^4I_{11/2}$	R_2-Y_1	1050.6	0.1118	372.855
	R_2-Y_2	1054.1	0.1118	369.137
	R_1-Y_1	1074.21	0.1118	348.697
	R_1-Y_2	1078.00	0.1118	345.015
	R_2-Y_4	1093.73	0.1118	330.270
	R_2-Y_5	1102.59	0.1118	333.331
	R_1-Y_4	1117.52	0.1118	309.517
	R_1-Y_6	1128.41	0.1118	300.593
$^4F_{3/2}\rightarrow {}^4I_{13/2}$	R_2-X_1	1318.34	0.6168	88.705
	R_1-X_2	1355.94	0.6168	81.512
	R_2-X_3	1366.86	0.6168	79.553
	R_2-X_4	*1387.54*	0.6168	76.009

Table of content:

Title

Authors

Affiliation

Keywords

Address of Corresponding author

Abstract

Introduction

Experimental

Results and Discussions

Conclusions

Acknowledgements

Caption of figures
References

Tables

Figures (total 11) in separate files (eps files)

Text (highlighting novelty of works) (see page 2)

Colour graphics (for graphical abstract) (see page 2)

Highlight of works

The morphological and size distribution change of Nd: Y_2O_3 nanoparticles due to calcination temperature influences the transparency of ceramic pellets.

Graphical abstract

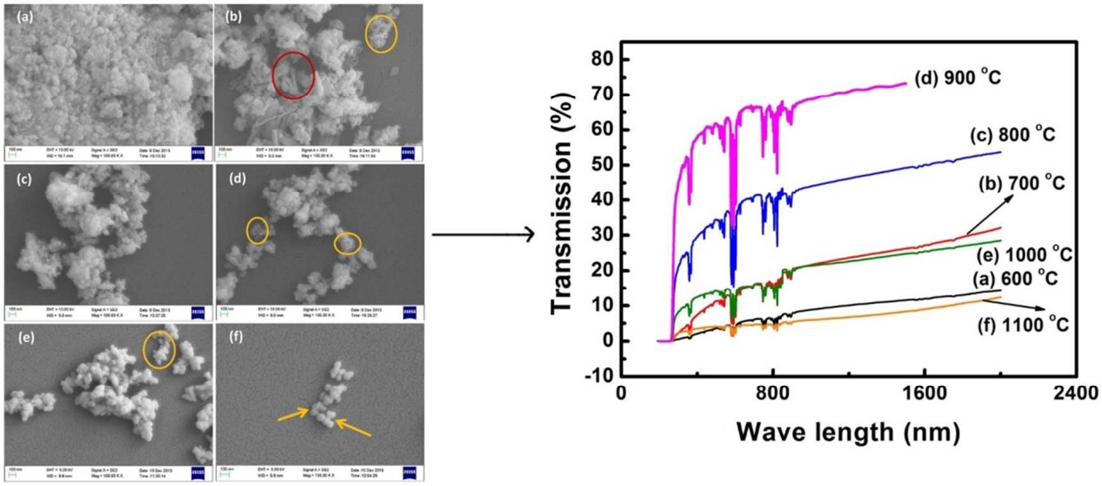

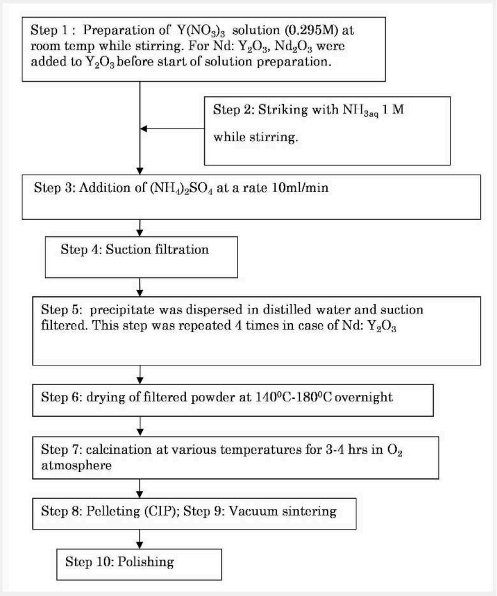

Step 1 : Preparation of $Y(NO_3)_3$ solution (0.295M) at room temp while stirring. For Nd: Y_2O_3, Nd_2O_3 were added to Y_2O_3 before start of solution preparation.

Step 2: Striking with NH_{3aq} 1 M while stirring.

Step 3: Addition of $(NH_4)_2SO_4$ at a rate 10ml/min

Step 4: Suction filtration

Step 5: precipitate was dispersed in distilled water and suction filtered. This step was repeated 4 times in case of Nd: Y_2O_3

Step 6: drying of filtered powder at 140^0C-180^0C overnight

Step 7: calcination at various temperatures for 3-4 hrs in O_2 atmosphere

Step 8: Pelleting (CIP); Step 9: Vacuum sintering

Step 10: Polishing

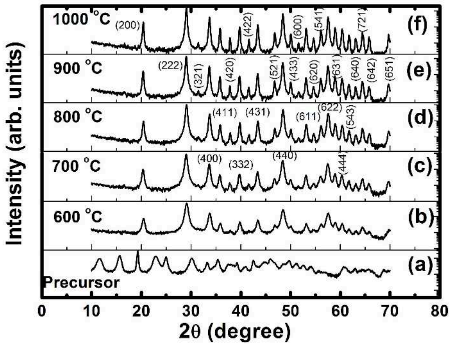
1000 °C
(200)
(422)
(600)
(541)
(721)
(f)
900 °C
(222)
(321)
(420)
(521)
(433)
(620)
(631)
(640)
(642)
(651)
(e)
800 °C
(411)
(431)
(611)
(622)
(543)
(d)
700 °C
(400)
(332)
(440)
(444)
(c)
600 °C
(b)
Precursor
(a)
Intensity (arb. units)
0
10
20
30
40
50
60
70
80
2θ (degree)

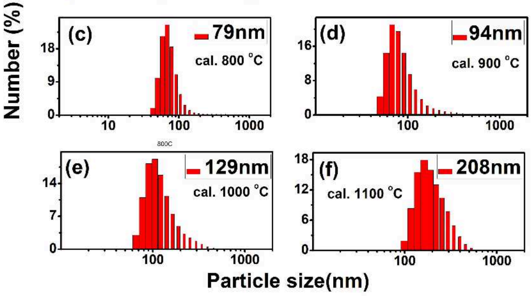
(a)
49nm
cal. 600 °C
30
20
10
0
10
100
1000
(b)
68nm
cal. 700 °C
20
10
0
100
1000
(c)
79nm
cal. 800 °C
18
9
0
10
100
1000
(d)
94nm
cal. 900 °C
16
8
0
100
1000
800C
(e)
129nm
cal. 1000 °C
14
7
0
100
1000
(f)
208nm
cal. 1100 °C
18
12
6
0
100
1000
Number (%)
Particle size(nm)

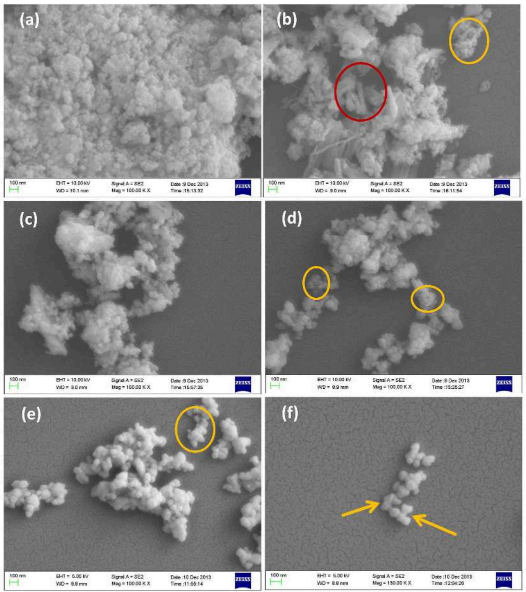
(a)
(b)
(c)
(d)
(e)
(f)

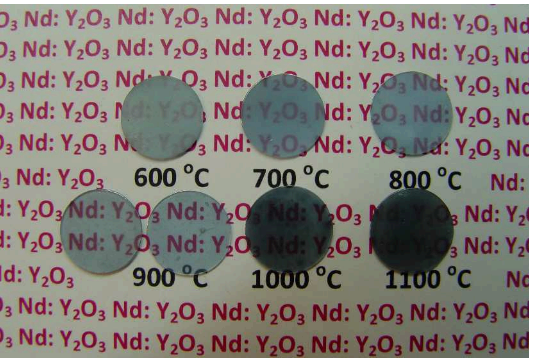
600 °C
700 °C
800 °C
900 °C
1000 °C
1100 °C

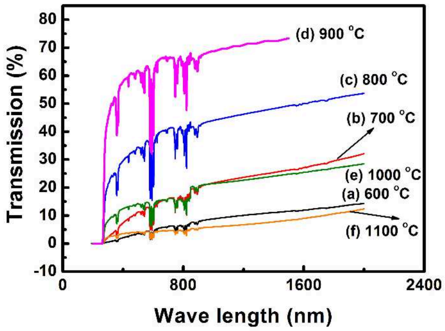
Transmission (%)
80
70
60
50
40
30
20
10
0
-10
0
800
1600
2400
Wave length (nm)
(d) 900 °C
(c) 800 °C
(b) 700 °C
(e) 1000 °C
(a) 600 °C
(f) 1100 °C

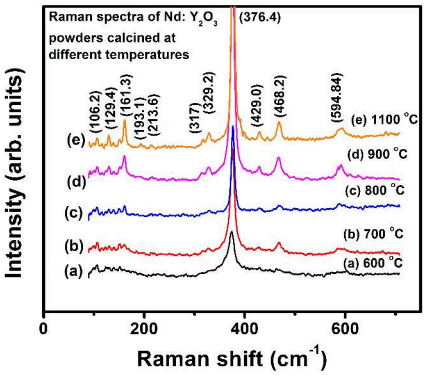
Raman spectra of Nd: Y2O3
powders calcined at
different temperatures
(376.4)
(106.2)
(129.4)
(161.3)
(193.1)
(213.6)
(317)
(329.2)
(429.0)
(468.2)
(594.84)
(e) 1100 °C
(d) 900 °C
(c) 800 °C
(b) 700 °C
(a) 600 °C
(e)
(d)
(c)
(b)
(a)
Intensity (arb. units)
0
200
400
600
Raman shift (cm-1)

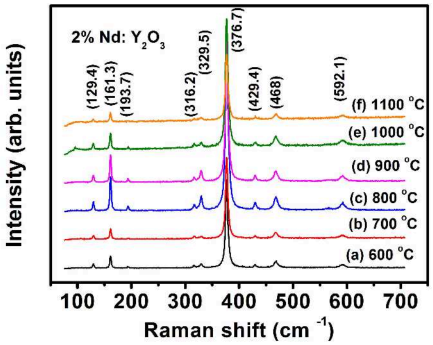
2% Nd: Y_2O_3
(129.4)
(161.3)
(193.7)
(316.2)
(329.5)
(376.7)
(429.4)
(468)
(592.1)
(f) 1100 °C
(e) 1000 °C
(d) 900 °C
(c) 800 °C
(b) 700 °C
(a) 600 °C
Intensity (arb. units)
100
200
300
400
500
600
700
Raman shift (cm $^{-1}$)

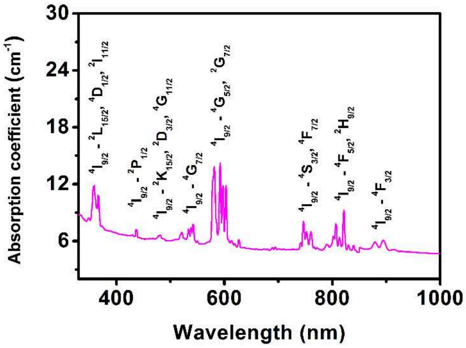
$^4I_{9/2}$ - $^2L_{15/2}$, $^4D_{1/2}$, $^2I_{11/2}$
$^4I_{9/2}$ - $^2P_{1/2}$
$^4I_{9/2}$ - $^2K_{15/2}$, $^2D_{3/2}$, $^4G_{11/2}$
$^4I_{9/2}$ - $^4G_{7/2}$
$^4I_{9/2}$ - $^4G_{5/2}$, $^2G_{7/2}$
$^4I_{9/2}$ - $^4S_{3/2}$, $^4F_{7/2}$
$^4I_{9/2}$ - $^4F_{5/2}$, $^2H_{9/2}$
$^4I_{9/2}$ - $^4F_{3/2}$
Absorption coefficient (cm^{-1})
30
24
18
12
6
400
600
800
1000
Wavelength (nm)

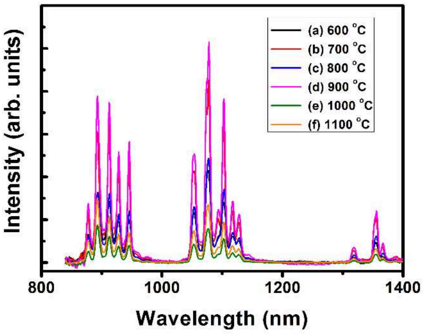
Intensity (arb. units)
Wavelength (nm)
800
1000
1200
1400
(a) 600 °C
(b) 700 °C
(c) 800 °C
(d) 900 °C
(e) 1000 °C
(f) 1100 °C

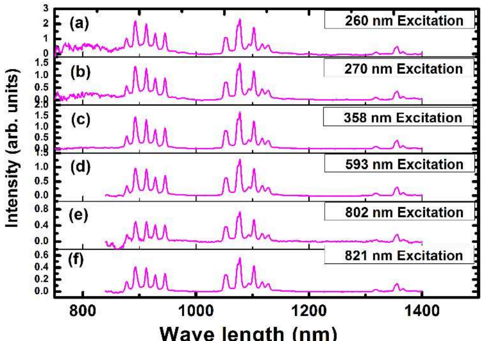
(a)
260 nm Excitation
(b)
270 nm Excitation
(c)
358 nm Excitation
(d)
593 nm Excitation
(e)
802 nm Excitation
(f)
821 nm Excitation
Intensity (arb. units)
3
2
1
0
1.5
1.0
0.5
0.0
2.0
1.5
1.0
0.5
0.0
1.5
1.0
0.5
0.0
0.8
0.4
0.0
0.6
0.4
0.2
0.0
800
1000
1200
1400
Wave length (nm)